Flexural behaviour of RC slabs strengthened with prestressed CFRP strips using different anchorage systems

Luís Correia [a], Tiago Teixeira [a†], Julien Michels [b], João A.P.P. Almeida [a], José Sena-Cruz [a*]

[a] ISISE, Dept. of Civil Engineering, Univ. of Minho, Azurém, 4800-058 Guimarães, Portugal

[b] Structural Engineering Research Laboratory, Swiss Federal Laboratories for Materials Science and Technology (Empa), Überlandstrasse 129, 8600 Dübendorf, Switzerland

* corresponding author: e-mail: jsena@civil.uminho.pt; tel.: (+351) 253 510 200; fax.: (+351) 253 510 217

Abstract

The Externally Bonded Reinforcement (EBR) technique using Carbon Fiber-Reinforced Polymers (CFRP) has been commonly used to strengthen concrete structures in flexure. The use of prestressed CFRP material offers several advantages well-reported in the literature. Regardless of such as benefits, several studies on different topics are missing. The present work intends to contribute to the knowledge of two commercially available systems that differ on the type of anchorage: (i) the Mechanical Anchorage (MA), and (ii) the Gradient Anchorage (GA). For that purpose, an experimental program was carried out with twelve slabs monotonically tested under displacement control up to failure by using a four-point bending test configuration. The effect of type of anchorage system (MA and GA), prestrain level (0 and 0.4%), width (50 mm and 80 mm) and thickness (1.2 mm and 1.4 mm) of the CFRP laminate, and the surface preparation (grinded and sandblasted) on the flexural response were the main studied parameters. Better performance was observed for the slabs: (i) with prestressed laminates, (ii) for the MA system, and (iii) with sandblasted surface preparation.

Keywords: A. Carbon-carbon composites (CCCs); B. Strength; D. Surface analysis; E. Surface treatments; CFRP EBR prestress systems

† Passed away on May 4th, 2015.

1. Introduction

Nowadays, Fibre Reinforced Polymer (FRP) materials and related strengthening techniques are well-known and used by the construction industry [1-7]. In the context of retrofitting Reinforced Concrete (RC) structures, Carbon FRP materials (CFRP) are used due to their superior performance, mainly higher stiffness, strength and fatigue life, almost no creep rupture and less susceptibility against aggressive environments [4-7]. From different attempts, one main strengthening technique has been selected [4-7]: the Externally Bonded Reinforcement (EBR). In this technique the FRP reinforcements are glued to the external surfaces of the elements to be strengthened. Typically epoxy adhesive are used as bond agent.

In some specific cases, the use of prestressed FRP materials for strengthening RC structures is convenient or even required. This technique presents several positive aspects since it combines the benefits of passive EBR FRP systems with the advantages associated with external prestressing, mainly [8]: (i) use of non-corrosive materials; (ii) deflection reduction; (iii) crack widths reduction and the onset of cracking is delayed; (iv) internal steel reinforcement strains are relieved; (v) higher fatigue failure resistance; (vi) more efficient use of the concrete and FRP; (vii) opposes stresses due to both dead and live loads; (viii) reduction risk of premature debonding failure between the FRP and concrete; (x) ultimate capacity can be further increased; (xi) it can be worked as a substitute of internal prestress that has been lost; (xii) shear capacity is increased by the longitudinal stresses induced by prestressed FRP laminates.

Laminates [9-13,16-18,25,26-29], sheets [14-15,20-23,25] and bars [20,29] are the most common prestressed FRP shapes, the former being the most prominent. Several systems have been proposed to induce a prestress in the FRP and can be divided in three categories [8]: (i) cambered prestressing systems; (ii) prestressing against an independent element; and, (iii) prestressing against the element to be strengthened. In spite of each one having advantages and disadvantages [8], the systems that apply the prestressing against the element to be strengthened have known so far the biggest success. Special end-anchorage systems are required at the ends of the prestressed FRP element to transfer the high shear stress developed from the reinforcement into the concrete substrate, in order to avoid a premature FRP peeling-off failure. From all the proposed systems, two of them have been used, mainly [31]: the mechanical anchorage (MA) fixed to the ends of the FRP reinforcement and the gradient anchorage (GA). Detailed information about these systems is given in section 2.3 of the present publication. Up to now, the majority of the studies focus on the development/improvement of the prestressing systems as well as the structural behaviour in terms of serviceability and ultimate resistance of the strengthened elements.

Surface preparation also plays a key role in the overall response of the strengthening systems. Some of the most common surface preparation methods are: grinding, brushing, scarifying, steel shotblasting, sandblasting, and bush-hammering. Each one of these methods presents advantages and disadvantages associated at several factors as the desired roughness, cost and processing time. Iovinella *et al*. [32] developed an interesting work on the influence of surface roughness on the bond of FRP materials to concrete. The study presents not only the investigations developed up to date, but also a detailed study performed on the influence of distinct surface treatments mainly, brushing, grinding, brush-hammering and sand blasting on bond strength and fracture energy of EBR strengthening systems. From this investigation Iovinella *et al*. [32] concluded that the bush-hammering and sand blasting were the most effective and in general the surface preparation significantly improves the roughness homogeneity along the surface, increasing the stability of results.

The present work aims at contributing to the existing knowledge on the flexural behaviour of RC slabs strengthened with prestressed CFRP strips. For that purpose, the performance of mechanical and the gradient end-anchorage systems were compared by means of an experimental program. Additionally, the effect of the prestrain level, the width and thickness of the CFRP laminate, as well as the surface preparation (grinded and sandblasted) on the flexural response were investigated.

2. Experimental Investigation

2.1. Experimental program, specimens and test configuration

The experimental program was composed of twelve slabs, divided into two series according to the surface preparation method (see **Table 1**): in series S1, composed of eight reinforced concrete (RC) slabs, the concrete surface region where the FRP reinforcement was installed was treated by means of grinding with a stone wheel, whereas in series S2 the surface preparation of the three RC slabs was performed by sand blasting. In both cases the main aim was to remove the weak concrete laitance layer and expose the aggregates of the substrate. Three slabs were used as control specimens (S1_REF1, S2_REF2 and S2_REF). In each series one slab was strengthened with a simple CFRP laminate strip according to the EBR technique without any prestressing (S1_L50×1.4_EBR and S2_L50×1.2_EBR). The remaining seven slabs were strengthened with one externally bonded prestressed CFRP laminate strip with either a mechanical anchorage (MA) or a gradient anchorage (GA). As it is shown in **Table 1**, all specimens are labelled with a generic denomination: X_LY_Z, where X is the specimen series (S1 or S2), Y is the cross-section geometry of the laminate strip in millimetres (50×1.4, 50×1.2 or 80×1.4) and Z is the type of anchorage (MA or GA) or the EBR slab identification.

The specimens' geometry and test configuration are shown in **Fig. 1**. The slabs have a total length of 2600 mm, the rectangular cross section is 600 mm wide and 120 mm thick. The upper and lower longitudinal inner reinforcement is composed of three steel bars with a diameter of 6 mm (3Ø6) and five bars with diameter 8 mm (5Ø8), respectively. To avoid shear failure of the slabs, steel stirrups Ø6 were installed at a spacing of 300 mm. Three types of CFRP laminates strips (50×1.2 mm^2, 50×1.4 mm^2 and 80×1.2 mm^2) with 2400 mm of length were used as external reinforcement.

In order to assess the service and ultimate behaviour of all specimens, monotonic tests up to failure were performed using a four point bending configuration. The instrumentation included 5 linear variable differential transducers (LVDT1 to LVDT5) to record the deflection along the longitudinal axis of the slab; 3 strain gauges (SG1 to SG3) with the aim of measuring the strain in the laminate and concrete; and 1 load cell used to measure the applied load (F). **Fig. 1** shows the position of each LVDT: three in the pure bending zone with the range of ±75 mm and a linearity error of ±0.10% and two between the supports and the applied load points with a range of ±25 mm and the same linearity error. The load cell used has a maximum measuring capacity of 200 kN and a linear error of ±0.05%. Two different strain gauge types were used: (i) two TML BFLA-5-3 strain sensors (SG1 and SG2) glued on the laminate surface at the mid-span and at the force application point; and, (ii) one TML PFL-30-11-3L strain sensor (SG3) for the measuring the concrete strain in the mid-span. All tests were carried out with a servo-controlled equipment under displacement control at a rate of 1.2 mm/min. The crack width evolution was measured during the test through a handheld USB microscope. This equipment consists on the VEHO VMS-004 D microscope, with a native resolution of 640×480 pixels and magnification capacity up to 400×. In the present experimental program, the crack width acquisition was done with a magnification factor of 20× up to predefined applied load.

It should be highlighted that, usually, in real applications cracks already exist at the moment of the FRP application. Consequently, the present experimental program does not totally reproduce the major part of the existing structures that require upgrading. However, critical aspects such post-cracking behaviour, yielding of the longitudinal reinforcements, ultimate load and failure modes can be well-captured by the present experimental program be representative of the expected real behaviour. Hence, the slabs' structural behaviour can be considered representative of the expected real behaviour. Additionally, with this work it is also possible to evaluate the effect of the FRP prestressing on crack initiation.

2.2. Material characterization

The material characterization included the evaluation of the mechanical properties of the materials involved in this experimental program, namely concrete, steel, CFRP laminate strip and epoxy adhesive.

Four batches (B1 to B4) were used to cast the RC slabs (see **Table 1**). Concrete characterization included evaluation of the modulus of elasticity and compressive strength through LNEC E397-1993:1993 [33] and NP EN 12390-3:2011 [34] recommendations, respectively. For each concrete batch six cylindrical specimens with 300 mm of height and 150 mm of diameter were used. **Table 2** shows the obtained results at the testing day. The average compressive strength of series S1 was about 53 MPa, whereas for the series S2 was about 40 MPa.

The tensile properties of the steel reinforcement were assessed throughout the NP EN ISO 6892-1:2012 [35] standard. A minimum of three specimens were used for each bar type. **Table 2** includes the Young's modulus (E_s) as well as the yield (f_y) and ultimate (f_u) strengths obtained from the tensile tests. The average value of the modulus of elasticity was about 212 GPa and 235 GPa for the lower longitudinal steel reinforcement in series S1 and S2, respectively. The steel of the longitudinal bars and stirrups has a denomination of A400 NR SD according to the NP EN 1992-1-1:2010 [36].

The CFRP laminate strips used in the experimental work consists of unidirectional carbon fibres held together by an epoxy vinyl ester resin matrix. Typically, this type of CFRP laminate presents smooth external surface and the fibre volume content is higher than 68% [37]. The modulus of elasticity (E_f) and tensile strength (f_f) were obtained from tests performed according to the ISO 527-5:1997 [39] standard. Four and six samples were used for S1 and S2 series, respectively. The obtained values, presented in **Table 2**, yielded to a Young's modulus that varied between 155 and 168 GPa and tensile strength in a range of 2375 to 2944 MPa.

The epoxy adhesive, produced by the same supplier as for the CFRP laminate, was used as bond agent to fix the reinforcements to the concrete substrate. This epoxy adhesive is a solvent free, thixotropic and grey two-component (Component A = resin, light grey colour and Component B = hardener, black colour). According to the manufacturer, after mixing the two components, the homogenized compound density is 1.70 to 1.80 g/cm^3 and has the following mechanical properties [38]: compressive strength >70 MPa; tensile E-modulus >7.1 GPa; shear strength >26 MPa; adhesive tensile strength to concrete or CFRP laminate >3 MPa (after 3 days of curing at 20 °C). In the scope of the present work the epoxy adhesive was not characterized. However, in a previous experimental program performed by two of the authors, after 7 days of curing at 22 ºC, a Young modulus of 7.7 GPa (CoV=3.1%) and a tensile strength of 20.7 MPa (CoV=9.9%) were obtained [40].

2.3. Strengthening procedures

As referred before, two distinct end-anchorage systems were investigated: (i) the mechanical anchorage (MA) which fix steel plates at the ends of the FRP reinforcement, and (ii) the gradient anchorage (GA). These commercially available systems from the same supplier as for the FRP reinforcement and adhesive, present several common equipment and step application procedures. The use of these systems comply the following main steps:

(i) The first step consists on the surface preparation of concrete substrate where the strip is applied. In the present experimental program two different methods were used: (i) gridding with stone wheel (**Fig. 2a – A1** and **Fig. 2b – A1**) and (ii) sand blasting (**Fig. 2a – A2** and **Fig. 2b – A2**). Afterwards, compressive air was used to clean the treated this region of the slab;

(ii) Several holes are drilled to accommodate temporary and permanent bolt anchors. GA system complies only temporary bolts, whereas for the case of MA system, six M16 8.8 permanent bolt anchors are used to fix each steel anchorage plate. HIT-HY 200-A® chemical bond agent was used to fix the bolts to concrete. Then, aluminium guides are placed in the right position to guide and fix the clamp units (**Fig. 2a – B** and **Fig. 2b – B**);

(iii) The clamp units are placed in-between the guides at each extremity of the slab;

(iv) The epoxy adhesive is prepared according to the requirements included in producer's technical datasheet and the CFRP laminate strip is cleaned with a solvent. Then, the adhesive is applied on the surface of the CFRP laminate as well as on the concrete surface region in contact with the laminate (**Fig. 2a – C** and **Fig. 2b – C**). A minimum of 2 mm of thickness of epoxy was used. The CFRP laminate strip is then placed in its final position and slightly pressed against the concrete substrate;

(v) The clamping units are closed and a dynamometric key is used to tighten the screws of the clamp units with a torque of 170 N·m (**Fig. 2a – D** and **Fig. 2b – D**);

(vi) For the case of MA system, anchor plates are slightly grinded with sandpaper and cleaned with a solvent before they are installed in their predefined location (**Fig. 2a – E**). The anchor plates of 270 mm × 200 mm × 10 mm, made of hard aluminium, have 6 holes of 18 mm diameter to accommodate the 6 permanent bolt anchors of 16 mm of diameter. In the case of GA, heating devices are placed in the gradient zone (**Fig. 2b – E**);

(vii) The aluminium frames are then placed on their predefined locations and fixed against the concrete with the anchors (**Fig. 2a – F** and **Fig. 2b – F**) in order to accommodate the hydraulic cylinder (**Fig. 2a – G** and **Fig. 2b – G**) for the application of the prestressing;

(viii) Finally, using a manual hydraulic pump, the prestress is applied to the CFRP laminate strip.

Once the CFRP is prestressed distinct procedures are followed for the case of the MA and the GA systems. In the MA system, by applying a torque of 150 N·m in each bolt anchor of the anchor plates (with a geometry of 270 mm × 200 mm × 20 mm), it is possible to increase the confinement level in this region and hence reducing the probability of the CFRP laminate sliding at the ends. Afterwards, by using additional fixing screws mounted in-between the frame and the clamp units, it is possible to block the prestressing system in order to avoid prestress losses during the curing of the epoxy. The strengthening application is concluded after approximately 24 hours, since after this time span the epoxy reaches a degree of curing at about 90% [42]. In the end, the equipment is removed (fixing screws, clamp units, guides and aluminium frames) and the temporary anchors and CFRP laminate outside of the anchor plates are cut off.

The GA system uses the adhesive's ability to cure fast at high temperatures and hence to create a non-mechanical anchorage [43]. For the present specimens, a 600 mm anchorage length was used, composed of 3 sectors (50/80 mm wide and 200 mm long each). During the application of the gradient method, all specimens were monitored in terms of applied force by the hydraulic cylinders and temperature at the distinct sectors composing the heating devices. The evolution of the temperature, jack force and strain over time is graphically represented on **Fig. 3** for the specimen S1_L50×1.4_GA: firstly it begins with a plateau of 160ºC during 15 minutes, followed by an exponential decrease during 20 minutes (down to 120ºC), and finally the cooling phase. In the following sector the same heating process is carried out 10 minutes after the beginning of the cooling phase. The releasing force in each step was equal to about 1/3 of the total applied force. This released occurred 15 minutes after the initiation of the cooling phase. After the first release a slight prestrain loss in the CFRP laminate (a variation at about 1.4%) can be observed, as depicted in **Fig. 3b**. This variation can be justified by the lower value of the modulus of elasticity of the epoxy adhesive due to the curing process [31]. Finally, it should be highlighted that the heating system does not change the mechanical performance of the CFRP strip. Material testing had shown that the CFRP remains undamaged during the heating process, and post-heating tensile strength is identical to the reference values [31].

In the prestressed specimens strain gauges were used to control the prestress level. The CFRP strip was prestressed up to an average prestrain of 0.4%. **Table 1** highlights the values of the registered prestrain and prestress force at the middle of the laminate at the end of the strengthening. The specimens were kept in lab environment after strengthening at least one month before testing.

Lastly, it should be stressed that the present pre-stressing systems can be used in sagging and hogging regions. For both cases a minimum camber is recommended. In spite of that, for the present case in order to facilitate the procedures, the strengthening was performed in upside down direction. However, for present work these effects were marginal since for the worst scenario (slabs S1_L80×1.2_MA and S1_L80×1.2_GA) the maximum camber was less than 1 mm and the maximum concrete tensile stress never exceeded its tensile strength.

2.4 Surface preparation

Considering the two different surface treatment methodologies applied at the concrete slab surfaces and in order to allow the identification of their influence on the obtained responses, the roughness of these distinct surfaces was measured. The procedure was based on the use of a laser sensor, whose main characteristics are presented in **Table 3**. The surfaces selected for the experimental characterization are representative of the three distinct types of surface treatments involved in the present research, which are the normal surface (without any treatment), the grinded surface, and the sand blasted surface. In **Fig. 4** it is possible to see the three different roughness of the material.

The laser sensor was coupled to a metallic plate, which was part of a mechanism conceived to produce a slow displacement at a constant rate, as well as to allow the displacement of the laser sensor during scanning at a parallel trajectory relatively to the scanned surface, as shown in **Fig. 5**. The displacement rate was 0.69 mm/s and the data acquisition rate was 120 Hz, leading to consecutive readings spaced of 0.00575 mm. Representative profiles of the three different surfaces are shown in **Fig. 6**. The representative profiles clearly distinguish the untreated surface and the treated surfaces, both the grinded and the sandblasted surfaces.

In this work several statistical indicators were considered to characterize the surface roughness, especially the average roughness, R_a, and the root mean square, R_q, as well as the peak and valley values of the samples. The average roughness and the root mean square can be determined using the equations (1) and (2), respectively. In these equations l_m is evaluation length, $z(x)$ is the profile height at position x, and n is the number of scan readings.

$$R_a = \frac{1}{l_m} \cdot \int_0^{l_m} z(x) \cdot dx \tag{1}$$

$$R_q = \sqrt{\frac{1}{n} \cdot \sum_{i=1}^{n} z_i^2} \tag{2}$$

The most common mathematical parameters used to characterize the roughness were computed for the three types of surfaces and are presented in **Table 4**. It is possible to verify that for the three different surfaces the

obtained values of roughness R_a show the expected trend, increasing in a reasonable fashion when departing from the smooth surface and arriving at the sandblasted slabs.

3. Results and discussion

3.1 Serviceability aspects

Deflections

The relationship between the applied force and the deflection at mid-span was monitored and it is represented in **Fig. 7**. As expected, the strengthening increased the stiffness of the composite system RC slab/CFRP strip and, as a consequence, reduced the deflection for a specific load level. **Table 5** summarizes the key results, for which the prestress level and the geometry of the CFRP strip were the influential factors.

Prestressing did not significantly change the stiffness of the elastic phase (K_I). However, substantial differences were observed in the stages after the crack initiation: firstly, cracking ($\delta_{cr,}$ F_{cr}) and steel yielding ($\delta_{y,}$ F_y) were delayed when compared with the non-prestressed specimens; and the stiffness after cracking (K_{II}) was higher in the strengthened slabs. Larger CFRP strips attract higher tensile forces and hence also induce higher system stiffness. Results show an average increase of 39%, 84% and 106% in the stiffness K_{II} of the S1 series prestressed specimens with 50×1.2 mm^2, 50×1.4 mm^2 and 80×1.2 mm^2 CFRP laminates, respectively. The same comparison shows an increase of 39% for the series S2 prestressed specimens.

In general, both prestressing strengthening techniques presented similar performances in terms of serviceability load/deflection up to yielding initiation.

Crack width

The crack width was monitored by a handheld USB microscope with a magnification factor of 20×. For that purpose three cracks were selected in the pure bending zone of each slab, two close to the point of loads and one at the mid-span. For every picture taken with the microscope, three measurements were performed in order to obtain the average crack width. **Fig. 8** plots the evolution of the average crack width *versus* the applied force. Results show that, for a specific load level, strengthened specimens exhibited lower crack widths when compared to the reference specimens. The MA and the GA systems presented similar results that could be foreseen due to their identical response in terms of force-deflection (at serviceability level). Resembling results were obtained for the series S1 and S2.

Crack pattern

The crack pattern was also evaluated at the end of each test. **Fig. 9** shows the crack pattern on the lateral surface of each tested slab and **Fig. 10** presents the values obtained in terms of average crack spacing. The results indicate that, in a general way, the crack spacing is reduced with the strengthening. This effect is more noticeable with the prestressed specimens: in series S1 the average distance between cracks of the five prestressed slabs was reduced to 79% of the reference specimens (S1_REF1 and S1_REF2); whereas for the prestressed specimens on series S2, the crack spacing reduction was equal to 36% of the value obtained with S2_REF. Through the crack pattern dawn in **Fig. 9** one can observe that the number of cracks in the pure bending zone is higher on the prestressed specimens.

Influence of the prestress

As expected, the overall behaviour of the prestressed specimens was considerably more satisfying than the un-prestressed ones in terms of ductility and load carrying capacities. Prestressing clearly improved the cracking and yielding initiation, stiffness and load carrying capacity. Even though the stiffness at the uncracked stage (K_I) was similar (prestressed *versus* un-prestressed) mainly due to the low level of strengthening ratio and level of prestrain that has been used, the cracking load was significantly higher: with series S1 an increase close to 55% was observed on specimens with the 50×1.4 mm^2 CFRP strip, whereas the cracking load duplicated in series S2 prestressed slabs. Similar observations can be made for the cracked stage (before yielding initiation). The load carrying capacity of prestressed slabs increased when compared with the unprestressed specimen. Results show that the ultimate carrying capacity growth was higher on series S1 (in between 60% and 107%) than on series S2 (within 30% and 53%).

Ultimately, **Fig. 11** shows the evolution of the CFRP and concrete strains at mid-span with the total force. Results also show a higher ultimate strain in the concrete for the prestressed specimens. Consequently, it can be stated that prestressing the CFRP laminates not only improved the slabs overall performance but also assured a better use of the materials. It should be also referred that a greater portion of the CFRP tensile capacity was engaged with the prestress (see **Fig. 11** and **Table 5**): on series S1 the strain at the ultimate load (F_{max}) was at least 93% higher than the observed on the S1_50×1.4_EBR; and on series S2 an increase of 53% and 95% was obtained for the S2_50×1.2_GA and S2_50×1.2_MA, respectively.

3.2 Ultimate state aspects

Failure modes

All the strengthened slabs seemed to fail by strip end debonding with the exception of the S2_50×1.2_MA specimen (see **Fig. 12-a**), that failed by FRP rupture in unidirectional tension when the CFRP strain at the mid-span was close to 1.48 %, as it is showed on **Table 5**.

In the remaining strengthened specimens, the failure started from one of the extremities and then shifted to the middle of the slab. An interfacial failure at the epoxy adhesive/CFRP laminate was observed at the anchorage zone of the MA and GA specimens (see **Fig. 12-b, Fig. 12-c** and **Fig. 12-d**). The remaining CFRP strip region seemed to simultaneously have an interfacial failure at epoxy adhesive/CFRP laminate and cohesive failure in the concrete. These interfacial failure modes observed may be justified by the higher compressive/tensile strength of the used concrete. In some of these specimens a layer of concrete was detached from the RC slab.

The S1_50×1.4_EBR seemed to have an interfacial failure between adhesive and the concrete (see **Fig. 12-e**), whereas S2_50×1.2_EBR slab's failure looked like an interfacial failure amongst the adhesive and the CFRP strip (see **Fig. 12-f**).

Gradient versus mechanical anchorage

Both GA and MA systems present a similar behaviour until steel yielding (see **Fig. 7**). After this point, the CFRP material is responsible to carry the additional loads as a result of the diminished contribution of the internal steel reinforcement (it must be pointed out that the steel reinforcement exhibits a quite small hardening modulus of elasticity). Consequently, the force increment supported by the CFRP laminate strip increased significantly at the onset of the yielding initiation, as shown in **Fig. 11a** and **b**.

The mechanical anchorage system exhibits two drop points on the F-δ curves (see **Fig. 7**) after the steel reinforcement yielding. This behaviour is related to the debonding initiation that occurred between the metallic plate anchors and the force application point. This statement is supported on the visual observation performed during and after the tests and by comparing e.g. the location of the drop points of the slab S1_L50×1.4_MA with the failure slab S1_L50×1.4_EBR (in **Fig. 7a**). From these two drop points, the CFRP laminate works unbonded to the substrate and as a cable fixed at both extremities (the metallic anchors). Consequently, the metallic anchors composing the MA system prevented a premature failure by debonding and allowed the slab to continue carrying load after that point.

From the experimental observations, the MA system has a better performance when compared with the GA system: MA specimens presented higher ultimate load capacity (9% to 16% increase depending on the laminate geometry) and a greater use of CFRP tensile capacity (an increase on ultimate strain in between 13% and 28% was observed) when compared with the GA series. It might be important to refer that the debonding of the CFRP strip always occurred firstly on the MA series, but, as mentioned before, the metallic plate anchors allowed the composite system RC slab/CFRP to continue carrying load. Lastly, it is important to stress out the importance of the specimen dimensions. A shorter span length involves that the total gradient zone occupies a larger relative portion of the complete laminate length. This leads to the situation where the end of the gradient anchorage is much closer to the loading point. The cracks that develop reach the anchorage zone much faster than for instance in case of a much slender beam with a higher span/depth ration. Aram *et al*. [44] reported about static loading tests where EBR strengthened beams exhibited an even higher load carrying capacity than the corresponding ones with a prestressed system and gradient anchorage. It was concluded that the short span had a negative effect on the anchorage capacity due to too high shear stresses in the end zone of the laminate. Similar conclusions can be drawn for the present investigation: a more slender slab with a larger span length might implicate more similar results for an MA or a GA, as the free length between the anchorage zones increases.

Influence of the FRP strip thickness

The thickness influence was evaluated through a performance comparison between S1_50×1.4_MA and S1_50x1.2_MA. As shown in **Fig. 7** both specimens presented an identical behaviour. The resemblance is due to the fact that both specimens failed by laminate end debonding at the metallic anchor. This type of failure is indeed governed by the maximum shear stress that this region can attain and, as a result, by the CFRP surface area in contact with the metallic anchor plate. For these two specimens the maximum shear stress resistance seemed to be influenced primarily by the width of the laminate. Remark that the laminate at the metallic anchor zone is confined by the pressure of this device due to the torque (150 N×m) applied in the six bolts (see **Fig. 2**). This confinement might actually diminish the strip thickness influence on the maximum carrying capacity of the composite system RC slab/CFRP strip.

Influence of the FRP strip width

A better performance was observed with the wider laminate. The specimens S1_50×1.2_MA and S1_80×1.2_MA were compared and it was clear that the behaviour of the second was better: higher cracking and steel yielding

forces, greater stiffness, and an increase on the ultimate caring capacity by 23%. Analysing the effect of the axial stiffness of the CFRP laminate on the stiffness of the slab at fully cracked state (K_{II}), it is clear that this relation matches well: the K_{II} of specimen S1_80×1.2_MA is 1.57 times higher than the one of the S1_50×1.2_MA and the axial stiffness of 80×1.2 is 1.54 higher than the 50×1.2 one. This inference is no longer found for the case of the ultimate load, since the failure is governed by laminate end debonding at the metallic anchor and, consequently the ultimate carrying capacity only increased by about 23% (S1_80×1.2_MA *versus* S1_50×1.2_MA). In fact, the maximum average shear stress in the CFRP laminate strip at the metallic anchorage zone was higher on the S1_50×1.2_MA (9.14 MPa) than on the S1_80×1.2_MA (7.40 MPa). This outcome implies that the shear stress is inconstant in the metallic anchor region and that laminates with smaller widths performed in this respect. Note that equal metallic anchors were used (270 mm × 200 mm) with the same torque per bolt (150 N×m) and, as a result of the laminate width, different confinement pressure levels were imposed (S1_50×1.2_MA – 20.83 MPa and S1_80×1.2_MA – 13.02 MPa).

Influence of the surface treatment

In the present experimental program the surface treatment was evaluated by comparing the specimens overall performance in series S1 (grinded) and series S2 (sand blasted). These two different surface treatment methodologies influence the surface roughness (see **Table 4**) and, consequently, the adherence between the epoxy adhesive and the concrete surface.

When the specimens S1_50×1.2_MA and S2_50×1.2_MA are compared, a better performance of the series S2 specimens can be observed: firstly, the S2_50×1.2_MA failed by a FRP rupture at its maximum tensile capacity (ultimate strain near 1.48%); and the debonding initiation, showed in **Fig. 7** as two drop points in the third branch of each F-δ curves, started earlier on the specimen with a grinded surface at the load close to 46 kN, while a value of 56 kN was registered for the sand blasted slab. Both slabs performed similarly in terms of cracking and yielding initiation, as they also had resembling stiffnesses (K_I and K_{II}).

The concrete plays a key role in the behaviour of each specimens in terms of ultimate carrying capacity, cracking and deflection development. For that reason, this comparison between series S1 and series S2 was made considering the improvement of the strengthening (relative to the reference specimens). S2_50×1.2_EBR indices that through sand blasting it was possible to obtain a better surface adherence. The ultimate force on this slab was 0.57 higher relative to the values registered on S2_REF. Regardless of the thicker laminate strip, the S1_50×1.4_EBR improved the ultimate carrying capacity by 38% when compared with the S1_REF1. **Fig. 12**

shows the failure mode reported on both slabs. It is clear that the surface's adherence was higher on series S2 as the S2_50×1.2_EBR debonding was in the interface epoxy adhesive/CFRP laminate instead of in the interface epoxy adhesive/concrete (S1_50×1.4_EBR).

Finally, it should be stressed that further investigation is required to verify the potential effect of surface roughness mixed together with the effect of different concrete strengths (series S1 *versus* S2).

4. Conclusions

This paper presents an experimental program in which the main objective was to assess the service and ultimate behaviour of two different types of anchorage systems in the context of the use of prestressed CFRP laminates strips applied according to the EBR technique: the mechanical anchorage (MA) and the gradient anchorage (GA). The obtained results allow to draw a certain number of conclusions:

- In general it was observed that, at service level, the strengthening (prestressed and non-prestressed) improved the slabs performance with lower deflections, crack width delay and lower crack spacing;
- A similar response was observed in both anchorage techniques. Yet, the metallic anchors composing the MA system prevented a premature failure by debonding and allowed the slabs to support higher ultimate loads and deflections;
- Eight of the nine strengthened specimens seemed to fail by strip end debonding. Only the S2_50×1.2_MA failed by FRP rupture at its maximum tensile capacity. The debonding failure started from one of the extremities and then shifted to the middle of the slabs;
- A greater use of the CFRP laminate strip tensile capacity was attained when prestressing was applied to the CFRP laminates. The average ultimate strain on the CFRP laminate increased by 132% and 74% with prestressing in series S1 and S2, respectively;
- The CFRP laminate width had a considerable influence on the general behaviour of the strengthened elements. The slab S1_80×1.2_MA showed an increase on the ultimate carrying capacity by 23%, greater stiffness (54%) and higher cracking (26%) and steel yielding forces (31%) when compared with the S1_50×1.2_MA. However, similar performance was observed for the strip with different thickness;
- All metallic anchors were confined with the same torque per bolt (150 N×m). As a result, wider laminates exhibit lower confinement pressures (S1_50×1.2_MA – 20.83 MPa *versus* S1_80×1.2_MA – 13.02 MPa). Results showed that the shear stress in the CFRP at the metallic anchor region is inconstant, as it was

possible to observe higher values on the S1_50×1.2_MA (9.14 MPa) than on the S1_80×1.2_MA (7.40 MPa).

- Concrete surfaces that have been sand blasted achieved a higher roughness and adherence than those grinded with a stone wheel. The performance improvement observed for each method of surface preparation fundaments this idea: series S2 specimens (sand blasted) showed relative higher ultimate loads and they did fail with higher CFRP strains.

Acknowledgements

This work is supported by FEDER funds through the Operational Program for Competitiveness Factors - COMPETE and National Funds through FCT - Portuguese Foundation for Science and Technology under the project FRPreDur - PTDC/ECM-EST/2424/2012. The authors also like to thank all the companies that have been involved supporting and contributing for the development of this study, mainly: S&P Clever Reinforcement Ibérica Lda, S&P Clever Reinforcement Company (Switzerland), Tecnipor - Gomes & Taveira Lda., Vialam – Indústrias Metalúrgicas e Metalomecânicas, Lda., Hilti Portugal-Produtos e Serviços, Lda. The first and second authors wish also to acknowledge the grants SFRH/BD/98309/2013 and SFRH/BD/94850/2013, respectively, provided by FCT.

References

[1] Bakis, C.; Bank, L.; Brown, V.; Cosenza, E.; Davalos, J.; Lesko, J.; Machida, A.; Rizkalla, S.; Triantafillou, T. (2002) "Fiber-Reinforced Polymer Composites for Construction - State-of-the-Art Review" *Journal of Composites for Construction*, 6(2): 73-87.

[2] Zoghi, M. - Ed. (2013) "The International Handbook of FRP Composites in Civil Engineering", CRC Press, 359-387 (ISBN 9780849320132).

[3] fib (2001) "Externally bonded FRP reinforcement for RC structures." Bulletin no. 14, The International Federation for Structural Concrete (fib), Lausanne, Switzerland, 130 pp.

[4] CNR-DT 200 (2004) "Guide for the design and construction of externally bonded FRP systems for strengthening existing structures", CNR - Advisory Committee on Technical Recommendations for Construction, Italy, 154 pp.

[5] ACI 440.2R-08 (2008) "Guide for the Design and Construction of Externally Bonded FRP Systems for Strengthening Concrete Structures." Reported by ACI Committee 440, American Concrete Institute, 80 pp.

[6] HB 305 (2008) “Design handbook for RC structures retrofitted with FRP and metal plates: beams and slabs”, Standards Australia GPO Box 476, Sydney, NSW 2001, Australia, 76 pp.

[7] CAN/CSA-S6-06 (2006) “Canadian highway bridge design code”, National Standard of Canada, Ontario, Canada, 800 pp.

[8] El-Hacha, R.; Wight R.G.; Green, M.F. (2001) “Prestressed fibre-reinforced polymer laminates for strenghtening structures.” *Progress in Structural Engineering and Materials*, 3: 111-121.

[9] Kotynia, R.; Walendziak, R.; Stoecklin, I.; Meier, U. (2011) “RC Slabs strengthened with Prestressed and Gradually Anchored CFRP Strips under Monotic and Cyclic Loading.” *Journal of Composites for Construction*, 15(2): 168-180.

[10] Motavalli, M.; Czaderski, C.; Pfyl-Lang, K. (2011) “Prestressed CFRP for Strengthening of Reinforced Concrete Structures: Recent Developments at Empa, Switzerland.” *Journal of Composites for Construction*, 15(2): 194-204.

[11] Mukherjee, A.; Rai, G.L. (2009) “Performance of reinforced concrete beams externally prestressed with fiber composites.” *Construction and Building Materials*, 23(2): 822-828.

[12] Yang, D.S.; Park, S.K.; Neale, K.W. (2009) “Flexural behaviour of reinforced concrete beams strengthened with prestressed carbon composites.” *Composite Structures*, 88(4): 497-508.

[13] Aram, M.R.; Czaderski, C.; Motavalli, M. (2008) “Effects of gradually anchored prestressed CFRP strips bonded on prestressed concrete beams.” *Journal of Composites for Construction*, 12(1): 25-34.

[14] Kim, Y.J.; Green, M.F.; Fallis, G.J. (2008) “Repair of bridge girder damaged by impact loads with prestressed CFRP sheets.” *Journal of Bridge Engineering*, 13(1): 15-23.

[15] Kim, Y.J.; Shi, C.; Bizindavyi, L.; Green, M.F. (2008) “Ductility and cracking behavior of prestressed concrete beams strengthened with prestressed CFRP sheets.” *Journal of Composites for Construction*, 12(3): 274-283.

[16] Woo, S.K.; Nam, J.W.; Kim, J.H.J.; Han, S.H.; Byun, K.J. (2008) “Suggestion of flexural capacity evaluation and prediction of prestressed CFRP strengthened design.” *Engineering Structures*, 30(12): 3751-3763.

[17] Czaderski, C.; Motavalli, M. (2007) “40-Year-old full-scale concrete bridge girder strengthened with prestressed CFRP plates anchored using gradient method.” *Composites Part B: Engineering*, 38(7-8): 878-886.

[18] Kim, Y.J.; Shi, C.; Bizindavyi, L.; Green, M.F. (2007) “Applying Prestressed CFRP Sheets to Restore Prestress Losses in Prestressed Concrete Beams.” *ACI Special Publication*, 245: 105-122.

[19] El-Hacha, R.; Elbadry, M. (2006) "Strengthening concrete beams with externally prestressed carbon fibre composites cables: experimental investigation." PTI Journal, 4(2): 53-70.

[20] Kim, Y.J.; Green, M.F.; Fallis, G.J. (2006) "Damaged bridge girder strengthening." *Concrete International*, 28(11): 47-52.

[21] El-Hacha, R.; Wight, R.G., Green, M.F. (2004) "Prestressed carbon fiber reinforced polymer sheets for strengthening concrete beams at room and low temperatures." *Journal of Composites for Construction*, 8(1): 3-13.

[22] El-Hacha, R.; Wight, R.G., Green, M.F. (2004) "Flexural behaviour of concrete beams strengthened with prestressed carbon fibre reinforced polymer sheets subjected to sustained loading and low temperature." *Canadian Journal of Civil Engineering*, 31(2): 239-252.

[23] Wu, Z.S.; Iwashita, K.; Hayashi, K.; Higuchi, T.; Murakami S.; Koseki Y. (2003) "Strengthening Prestressed-Concrete Girders with Externally Prestressed PBO Fiber Reinforced Polymer Sheets." *Journal of Reinforced Plastics and Composites*, 22(14): 1269-1286.

[24] Wight, R.G.; Green, M.F.; Erki, M.A. (2001) "Prestressed FRP sheets for poststrengthening reinforced concrete beams." *Journal of Composites for Construction*, 5(4): 214-220.

[25] Svecova, D.; Razaqpur, A.G. (2000) "Flexural Behavior of Concrete Beams Reinforced with Carbon Fiber-Reinforced- Polymer (CFRP) Prestressed Prisms." *ACI Structural Journal*, 97(5): 731-738.

[26] Lees, J.M.; Burgoyne, C.J. (1999) "Experimental study of influence of bond on flexural behavior of concrete beams pretensioned with aramid fiber reinforced plastics." *ACI Structural Journal*, 96(3): 377-385.

[27] Quantrill, R.J.; Hollaway, L.C. (1998) "The flexural rehabilitation of reinforced concrete beams by the use of prestressed advanced composite plates." *Composites Science and Technology*, 58(8): 1259-1275.

[28] Bryan, P.E.; Green, M.F. (1996) "Low temperature behaviour of CFRP prestressed concrete beams." *Canadian Journal of Civil Engineering*, 23(2): 464-470.

[29] Meshgina, P.; Choib, K.K.; Taha, M.M.R. (2009) "Experimental and analytical investigations of creep of epoxy adhesive at the concrete–FRP interfaces." *International Journal of Adhesion & Adhesives*, 29: 56–66.

[30] Huang, J, Huang, P., Zheng, X., (2015) "Experimental study of prestress losses of RC beams strengthened with prestress FRP". Journal of building structures, 36: 85-91.

[31] Michels, J.; Sena-Cruz, J.; Czaderski, C.; Motavalli, M. (2013) "Structural strengthening with prestressed CFRP strips with gradient anchorage." *Journal of Composites for Construction*, 17(5):651–661.

[32] Iovinella, I.; Prota, A.; Mazzotti, C. (2013) "Influence of surface roughness on the bond of FRP laminates to concrete", *Construction and Building Materials*, 40: 533–542.

[33] LNEC E397-1993. (1993) “Concrete - Determination of the elasticity Young modulus under compression”. Portuguese specification from LNEC.

[34] NP EN 12390-3. (2011) “Testing hardened concrete. Part 3: Compressive strength of test specimens”. IPQ - Instituto Português da Qualidade, Caparica.

[35] NP EN ISO 6892-1. (2012) “Metallic Materials. Tensile Testing. Part 1: Method of test at room temperature”. IPQ - Instituto Português da Qualidade, Caparica.

[36] NP EN 1992-1-1. (2010) “Design of concrete structures. Part 1-1: General rules and rules for buldings” . IPQ - Instituto Português da Qualidade, Caparica.

[37] S&P. (2014) “CFRP Laminates, Technical datasheet”. Seewen, Switzerland, 6 pp.

[38] S&P. (2013) “Resin 220 epoxy adhesive, Technical datasheet”. Seewen, Switzerland, 3 pp.

[39] ISO 527-5. (1997) “Plastics — Determination of tensile properties — Part 5: Test conditions for unidirectional fibre-reinforced plastic composites”. ISO - International Organization for Standardization, Genève, 11 pp.

[40] Sena-Cruz, J.; Michels, J.; Czaderski, C.; Motavalli, M. (2012) “Mechanical behavior of epoxy adhesives cured at high temperatures” Technical Report no. 880163, Empa, Switzerland, 2012, 30 pp.

[41] S&P. (2010) “Pre-stressed S&P Laminates CFK. Manual for applicators. Technical Report”. HüM/03.04.2011, 20 pp.

[42] Fernandes, P.; Granja, J.; Benedetti, A.; Sena-Cruz, J.; Azenha, M. (2015) “Quality control and monitoring of NSM CFRP systems: E-modulus evolution of epoxy adhesive and its relation to the pull-out force” *Composites Part B*, 75: 95–103.

[43] Michels, J.; Czaderski, C.; El-Hacha, R.; Brönnimann, R.; Motavalli, M. (2012) “Temporary bond strength of partly cured epoxy adhesive for anchoring prestressed CFRP strips on concrete” *Composite Structures*, 94: 2667–2676.

[44] Aram, M.R.; Czaderski, C.; Motavalli, M. (2008) “Effects of gradually anchored prestressed CFRP strips bonded on prestressed concrete beams.” *Journal of Composites for Construction*, 12(1): 25–34.

Nomenclature

E_a	Average tensile modulus of epoxy adhesive
E_c	Average modulus of elasticity of concrete at slab testing day
E_f	Average elastic modulus of CFRP laminate
E_s	Average Young modulus of steel bars
f_c	Average compressive strength on cylinder 150mm/300mm of concrete at slab testing day
F_{cr}	Force at crack initiation
f_a	Average tensile strength of epoxy adhesive
f_f	Average tensile strength of CFRP laminate
F_{max}	Maximum force
f_t	Average ultimate strength of steel bars
f_y	Average yield strength of steel bars
F_y	Force at yielding initiation
K_I	Stiffness of the slab at uncracked state
K_{II}	Stiffness of the slab at fully cracked state
δ_{cr}	Mid-span displacement at cracking load F_{cr}
δ_{max}	Mid-span displacement at ultimate load F_{max}
δ_y	Mid-span displacement at yielding load F_y
ε_{fmax}	CFRP strain at F_{max}
ε_{fp}	CFRP initial strain
φ_y	Mid-span curvature at yielding load Fy
φ_{max}	Mid-span curvature at ultimate load F_{max}

List of Tables

Table 1: Experimental program

Table 2: Material characterization (average values)

Table 3: Properties of the laser sensor Sick OD2-P50W10A0

Table 4: Results from the roughness assessment

Table 5: Main results

Table 1: Experimental program

Specimen	**Laminate geometry** [mm^2]	**Initial strain, ε_{fp}** [$\times 10^{-3}$]	**Prestress force** [kN]	**Anchorage system**	**Batch**	**Type of surface preparation**
Series S1						
S1_REF1	-	-	-	-	B1	GD
S1_L50×1.4_EBR	50×1.4	0.00	-	-		
S1_L50×1.4_MA	50×1.4	3.98	43.1	MA		
S1_L50×1.4_GA	50×1.4	4.05	43.9	GA		
S1_REF2	-	-	-	-	B2	
S1_L50×1.2_MA	50×1.2	4.19	42.2	MA	B3	
S1_L80×1.2_MA	80×1.2	3.99	63.1	MA	B2	
S1_L80×1.2_GA	80×1.2	4.06	64.1	GA		
Series S2						
S2_REF	-	-	-	-	B4	SB
S2_L50×1.2_EBR	50×1.2	0.00	-	-		
S2_L50×1.2_MA	50×1.2	4.23	41.6	MA		
S2_L50×1.2_GA	50×1.2	3.98	39.2	GA		

Notes: GA = Gradient Anchorage; MA = Mechanical Anchorage; GD = Grinding; SB = Sand Blasting.

Table 2: Material characterization (average values)

Concrete

Series	**Batch**	E_c [GPa]	f_c [MPa]
S1	B1	32.2 (7.5%)	53.4 (4.3%)
	B2	32.6 (0.1%)	57.4 (3.0%)
	B3	30.7 (n.a.)	49.5 (3.1%)
S2	B4	30.0 (n.a.)	40.2 (0.7%)

Steel

Series	**Bar Type**	E_s [GPa]	f_y [MPa]	f_t [MPa]
S1	Ø6	209.5 (8.5%)	579.3 (3.3%)	669.7 (1.7%)
	Ø8	212.8 (9.7%)	501.4 (5.9%)	593.9 (3.9%)
S2	Ø6	206.9 (0.4%)	519.4 (6.1%)	670.2 (5.1%)
	Ø8	235.1 (4.6%)	595.9 (4.1%)	699.0 (2.1%)

CFRP

Series	**Geometry** [mm^2]	E_f [GPa]	f_f [MPa]
S1	50×1.2	167.7 (2.9%)	2943.5 (1.6%)
	50×1.4	154.8 (4.6%)	2457.1 (1.2%)
	80×1.4	164.6 (0.2%)	2455.3 (5.0%)
S2	50×1.2	164.0 (3.1%)	2374.9 (2.5%)

Note: the values between parentheses are the corresponding coefficients of variation (CoV).

Table 3: Properties of the laser sensor Sick OD2-P50W10A0

Parameter	**Value**
Resolution	5 µm
Repeatability	15 µm
Linearity	± 20 µm
Light spot dimension	0.5 mm × 1.0 mm (at 50 mm)

Table 4: Results from the roughness assessment

Roughness parameter [mm]	**Smooth**	**Grinded**	**Sandblasted**	
			Slab A	Slab B
Arithmetic average of absolute values, R_a	0.021	0.046	0.081	0.099
Root mean squared, R_q	0.026	0.060	0.110	0.135
Maximum valley depth, R_v	-0.076	-0.228	-0.577	-0.636
Maximum peak height, R_p	0.090	0.173	0.248	0.405
Maximum height of the profile, R_t	0.166	0.401	0.826	1.042

Table 5: Main results

Specimen	Stiffness		Crack initiation		Yielding			Ultimate				Efficiency and ductility parameters			FM
	K_I	K_{II}	δ_{cr}	F_{cr}	δ_y	φ_y	F_y	δ_{max}	F_{max}	φ_{max}	ε_{fmax}[(c)]				
	[kN/mm]	[kN/mm]	[mm]	[kN]	[mm]	[10^{-3} m^{-1}]	[kN]	[mm]	[kN]	[10^{-3} m^{-1}]	[10^{-3}]	F_{max}/F_y	δ_{max}/δ_y	φ_{max}/φ_y	
Series S1															
S1_REF1	4.47	0.79	2.47	11.04	15.74	-	21.50	100.02[(a)]	25.42[(b)]	-	-	-	-	-	-
S1_L50×1.4_EBR	8.98	1.21	1.64	14.73	17.00	31.59	33.30	20.47	35.06	36.42	4.64	1.05	1.20	1.15	D
S1_L50×1.4_MA	9.81	1.43	2.25	22.07	17.80	36.66	44.32	69.84	61.76	86.81	11.97	1.39	3.92	2.37	D
S1_L50×1.4_GA	10.60	1.48	2.25	23.84	18.86	41.48	48.35	34.39	56.02	65.20	10.29	1.16	1.82	1.57	D
S1_REF2	4.47	0.87	2.49	11.12	15.96	-	22.90	100.00[(a)]	26.94[(b)]	-	-	-	-	-	-
S1_L50×1.2_MA	9.02	1.22	2.53	22.81	20.57	45.64	44.89	73.23	59.09	91.15	12.53	1.32	3.56	2.00	D
S1_L80×1.2_MA	11.44	1.88	2.51	28.71	18.43	39.40	58.67	48.62	72.58	70.03	10.13	1.24	2.64	1.78	D
S1_L80×1.2_GA	9.92	1.71	2.88	28.56	20.31	37.31	58.31	30.61	66.21	53.02	8.96	1.14	1.51	1.42	D
Series S2															
S2_REF	11.10	0.92	0.71	7.88	18.90	-	24.54	100.00[(a)]	28.07[(b)]	-	-	-	-	-	-
S2_L50×1.2_EBR	12.49	1.13	0.68	8.49	25.87	43.88	37.05	40.69	43.98	71.34	7.56	1.19	1.57	1.63	D
S2_L50×1.2_MA	9.82	1.31	1.82	17.87	26.88	44.81	50.58	84.78	67.46	77.26	14.76	1.33	3.15	1.72	F
S2_L50×1.2_GA	10.43	1.24	1.55	16.16	29.04	52.60	50.20	43.31	57.38	76.49	11.58	1.14	1.49	1.45	D

Notes: D = Debonding; F = CFRP tensile failure; [(a)] these beams reached the maximum pre-defined deflection without failing; [(b)] values for the mid-span deflection of 100 mm; [(c)] The maximum CFRP strain did not necessarily occur at the mid-span.

List of Figures

Fig. 1: Specimen's geometry and test setup. Note: all units are in millimetres.

Fig. 2: Strengthening procedures: (a*)* mechanical anchorage system; (b) gradient anchorage.

Fig. 3: Evolution of the temperature, jack force and CFRP strain on S2_50×1.2_GA over time: (a) temperature in the heating *elements* $T_{h,i}$ and in the epoxy *adhesive* $T_{a,j}$; (b) hydraulic jack *force* F and mid-span CFRP *strain* **εf.**

Fig. 4: Different roughness of concrete surfaces: (a) smooth (before any treatment); (b) grinded treatment; (c) sandblasted treatment.

Fig. 5: Setup details about the device used to control de displacement of the sensor.

Fig. 6: Different roughness of concrete surfaces: (a) smooth (before any treatment); (b) grinded treatment; (c) sandblasted treatment.

Fig. 7: Total force *versus* mid-span deflection: (a) series S1; (b) series S2.

Fig. 8: Crack width evolution of: (a) Series S1; (b) Series S2.

Fig. 9: Crack pattern at the end of the test of each slab.

Fig. 10: Crack spacing of each slab of: (a) Series S1 and (b) Series S2.

Fig. 11: Total force *versus* CFRP/concrete strain: (a) Mid-span CFRP strain in Series S1; (b) Mid-span CFRP strain in Series S2; (c) Mid-span concrete strain in Series S1; (d) Mid-span concrete strain in Series S2.

Fig. 12: Typical failure modes: (a) FRP rupture in unidirectional tension (S2_50×1.2_MA); (b) interfacial failure at the epoxy adhesive/CFRP laminate (S2_50×1.2_GA); (c) detail at the anchorage zone (S2_50×1.2_GA); (d) detail of the CFRP strip's extremity (S2_50×1.2_GA); (e) interfacial failure between adhesive and the concrete (S1_50×1.4_EBR); (f) interfacial failure amongst the adhesive and the CFRP strip (S2_50×1.2_EBR).

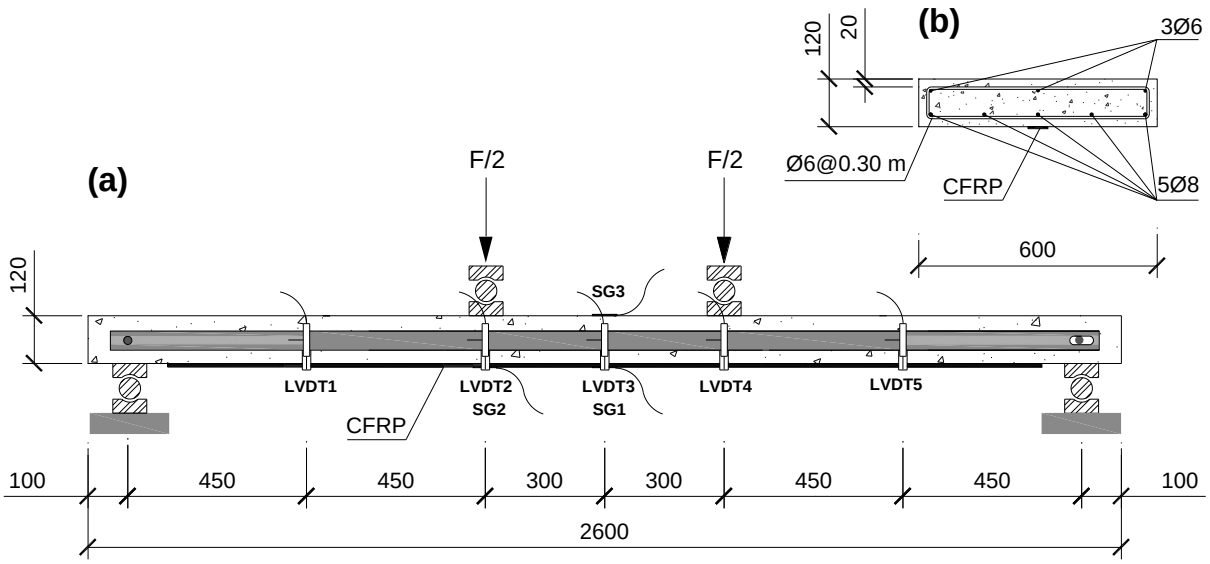

Fig. 1: Specimen's geometry and test setup. Note: all units are in millimetres.

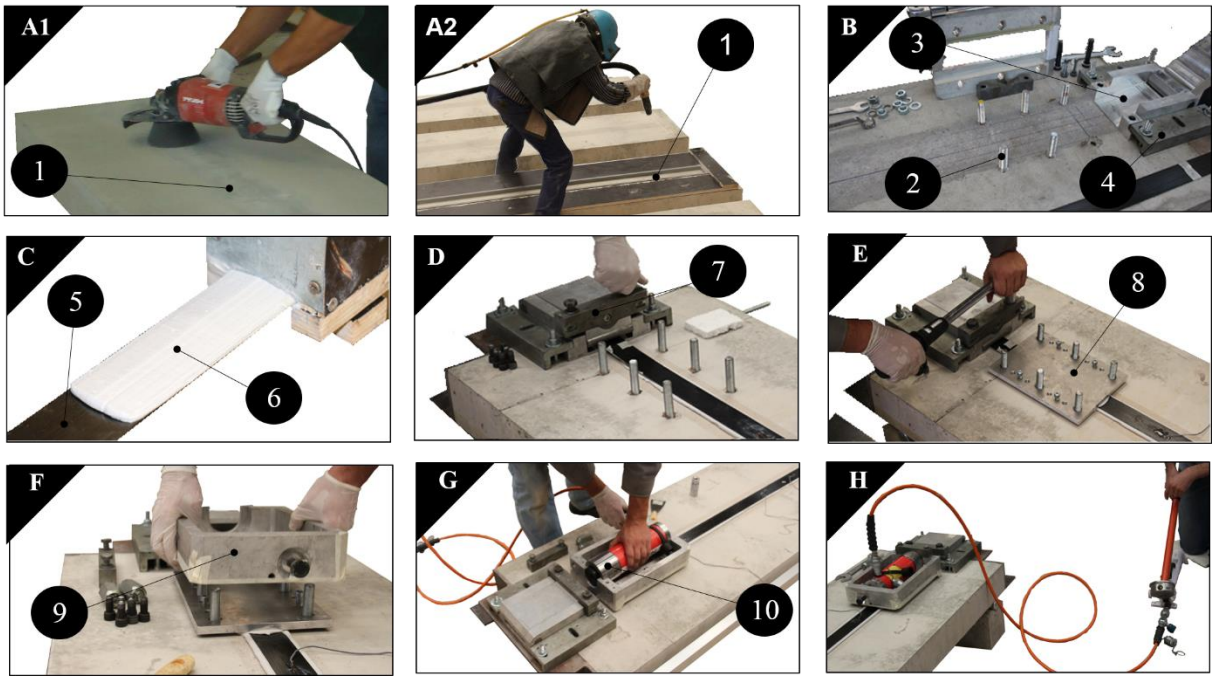

(a)

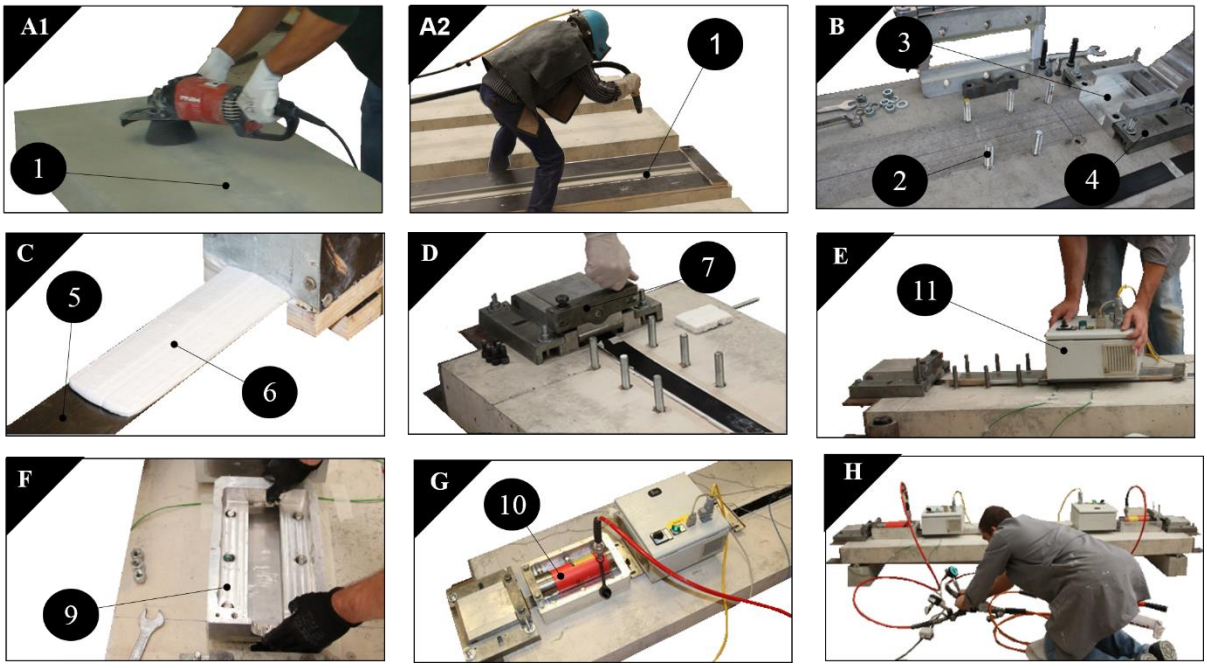

(b)

Legend: 1 – Concrete substrate; 2 – Anchor bolts; 3 – Clamp unit; 4 – Guides; 5 – CFRP laminate; 6 – Epoxy adhesive; 7 – Clamp unit closed; 8 – Metallic anchor; 9 – Aluminium frame; 10 – Hydraulic cylinder; 11 – Heating device.

Fig. 2: Strengthening procedures: (a) mechanical anchorage system; (b) gradient anchorage.

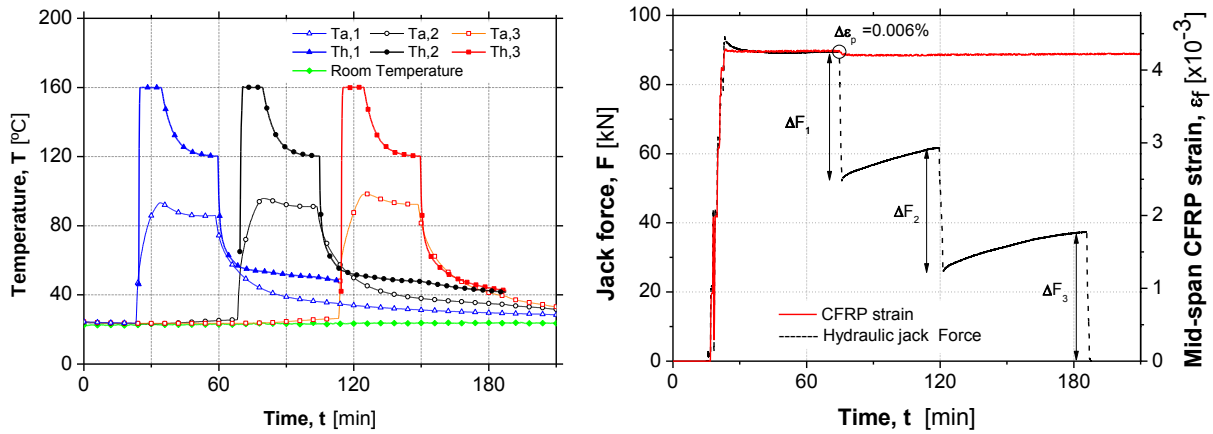

(a) (b)

Fig. 3: Evolution of the temperature, jack force and CFRP strain on S2_50×1.2_GA over time: (a) temperature in the heating elements $T_{h,i}$ and in the epoxy adhesive $T_{a,j}$; (b) hydraulic jack force F and mid-span CFRP strain ε_f.

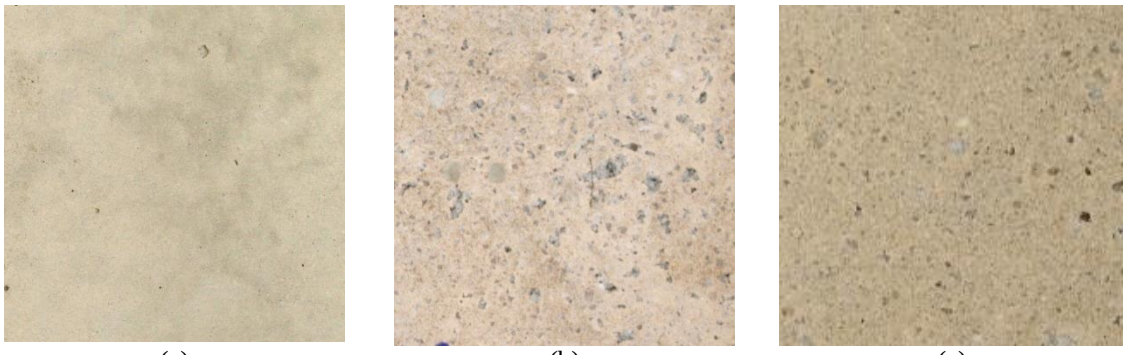

(a) (b) (c)

Fig. 4: Different roughness of concrete surfaces: (a) smooth (before any treatment); (b) grinded treatment; (c) sandblasted treatment.

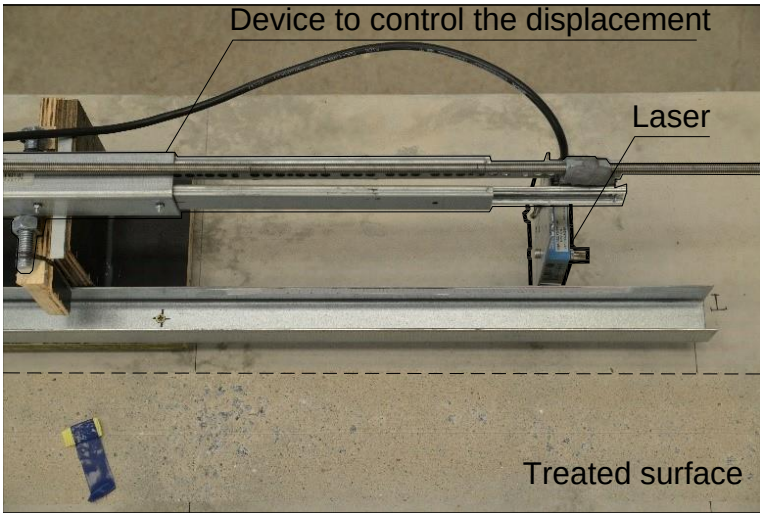

Fig. 5: Setup details about the device used to control de displacement of the sensor.

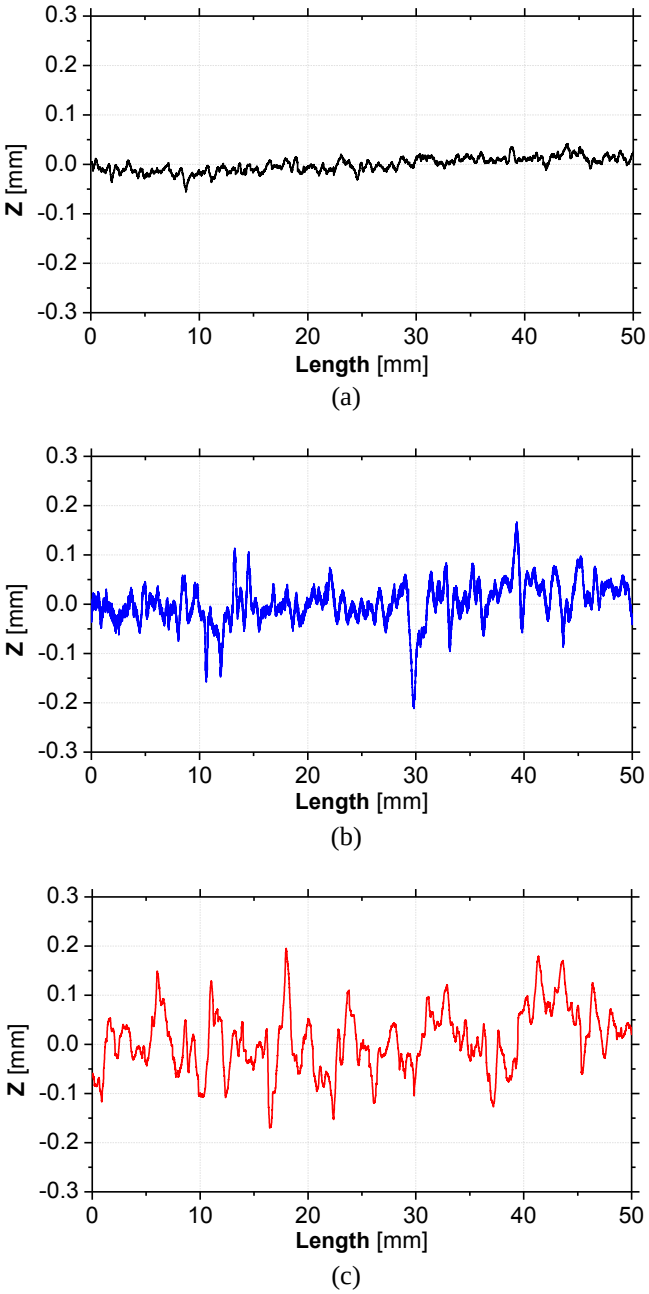

Fig. 6: Different roughness of concrete surfaces: (a) smooth (before any treatment); (b) grinded treatment; (c) sandblasted treatment.

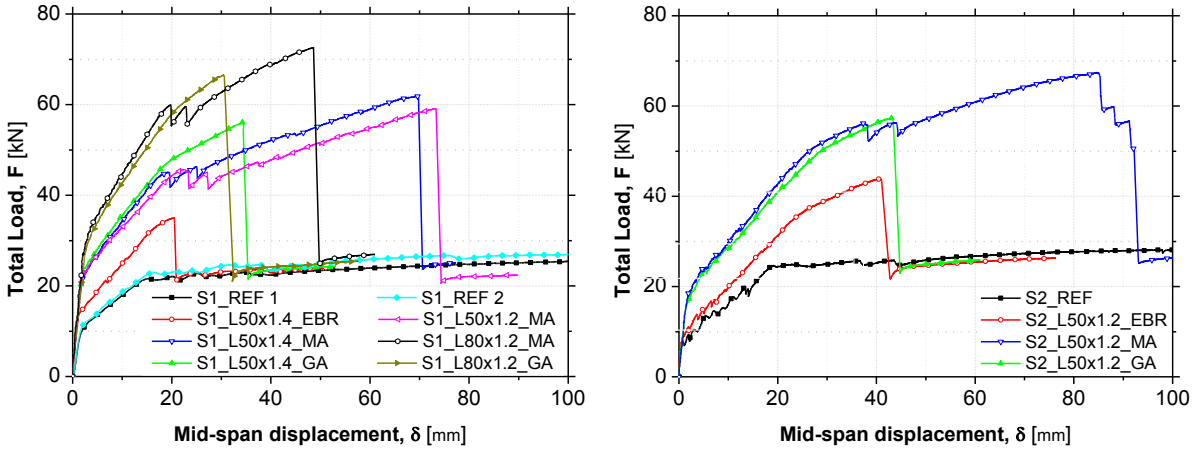

(a) (b)

Fig. 7: Total force *versus* mid-span deflection: (a) series S1; (b) series S2.

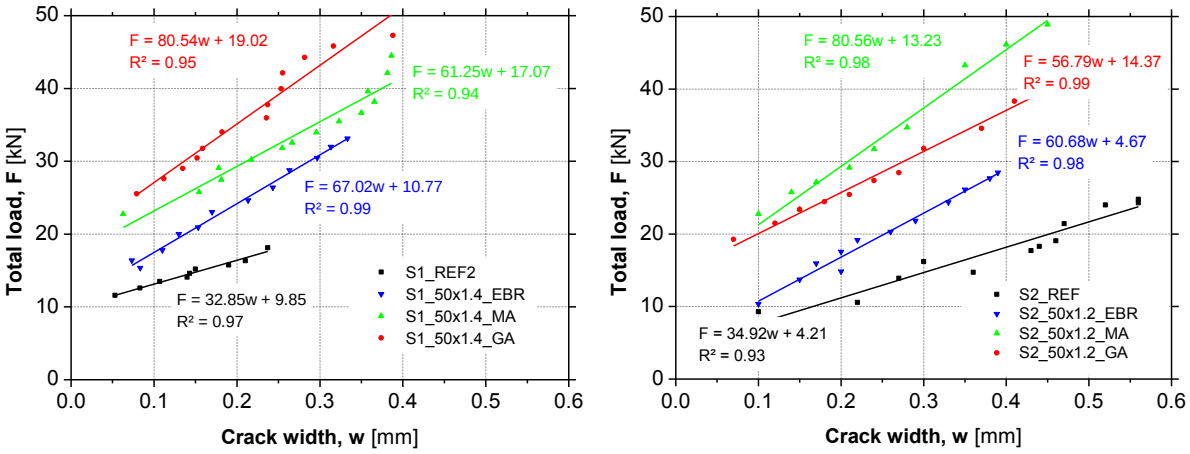

(a) (b)

Fig. 8: Crack width evolution of: (a) Series S1; (b) Series S2.

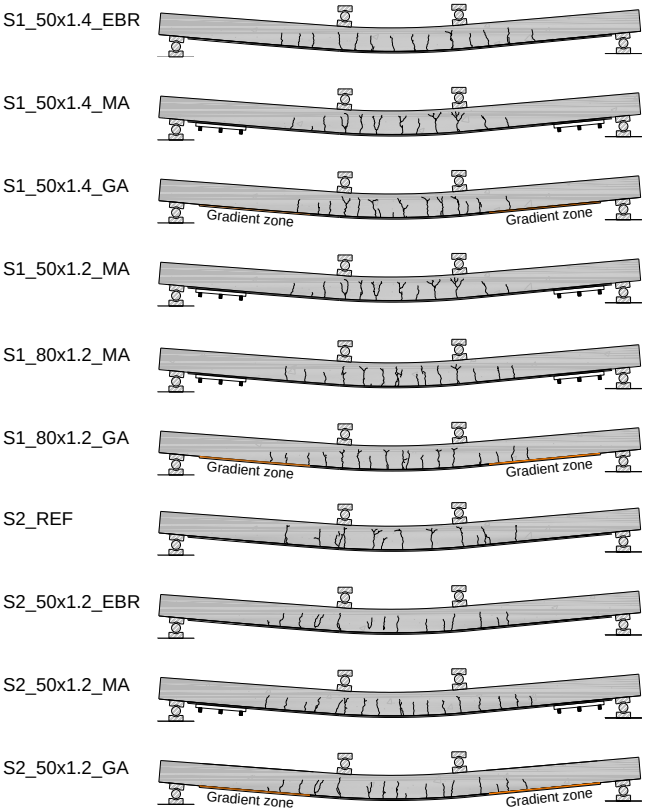

Fig. 9: Crack pattern at the end of the test of each slab.

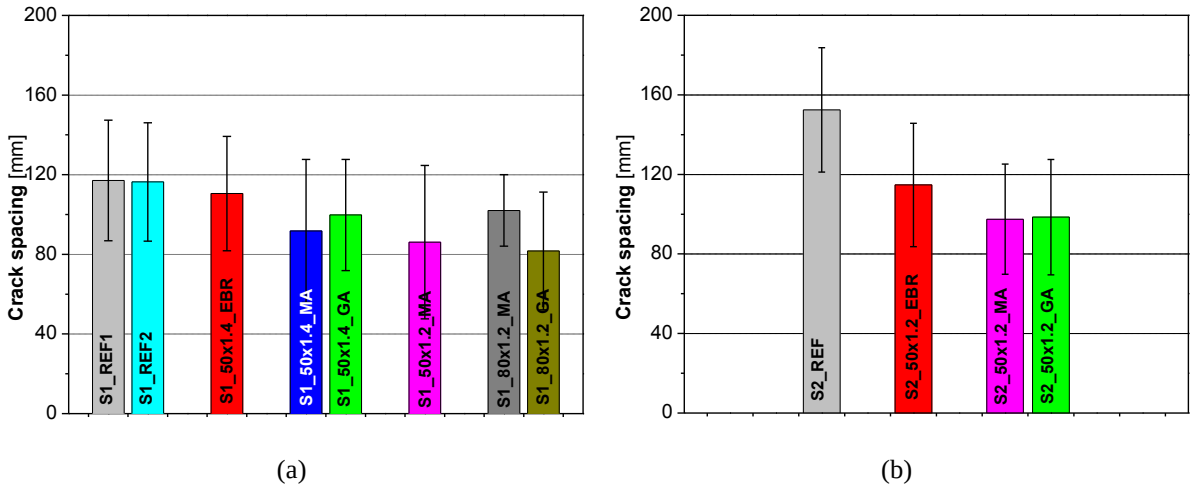

Fig. 10: Crack spacing of each slab of: (a) Series S1 and (b) Series S2.

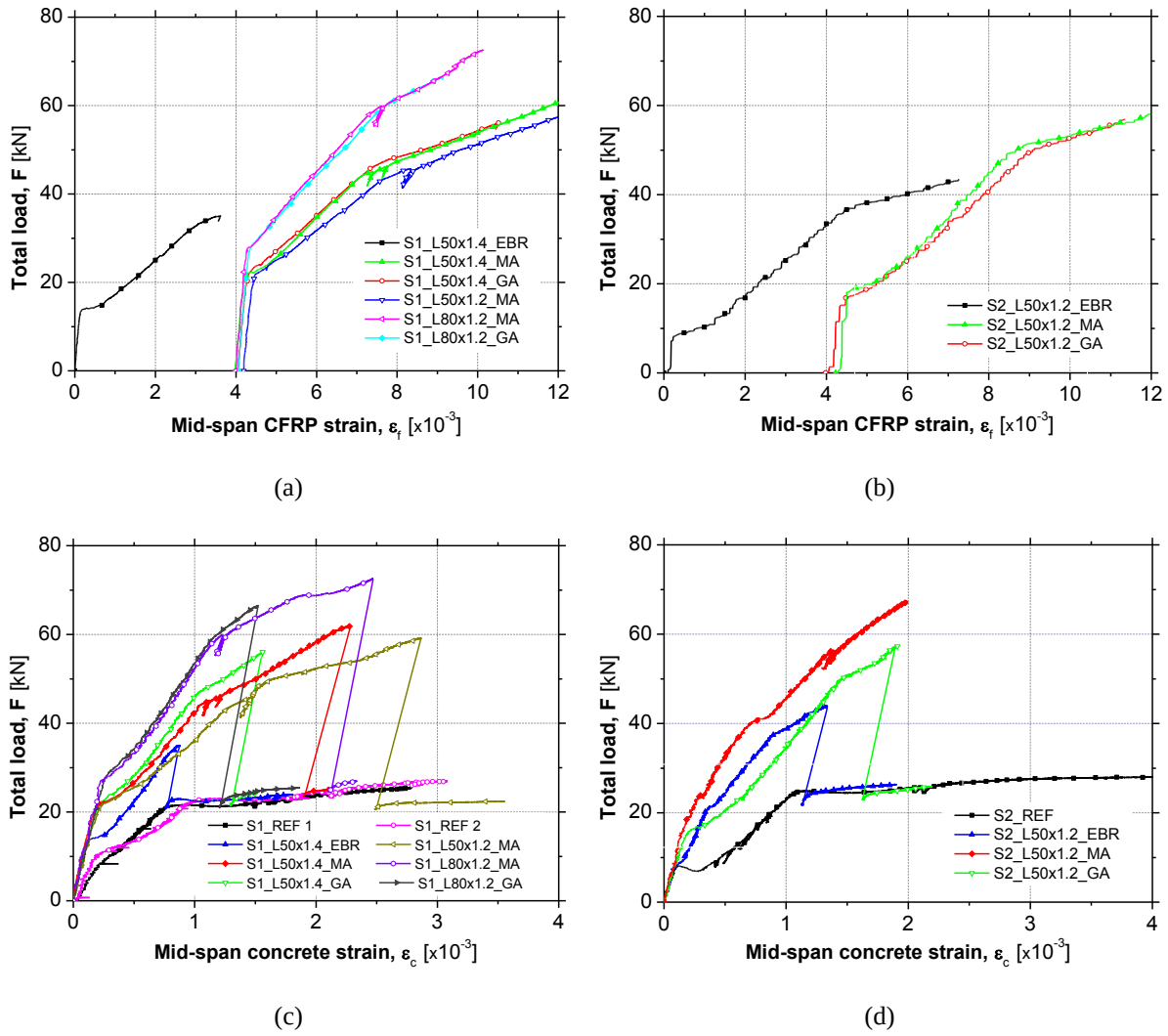

Fig. 11: Total force *versus* CFRP/concrete strain: (a) Mid-span CFRP strain in Series S1; (b) Mid-span CFRP strain in Series S2; (c) Mid-span concrete strain in Series S1; (d) Mid-span concrete strain in Series S2.

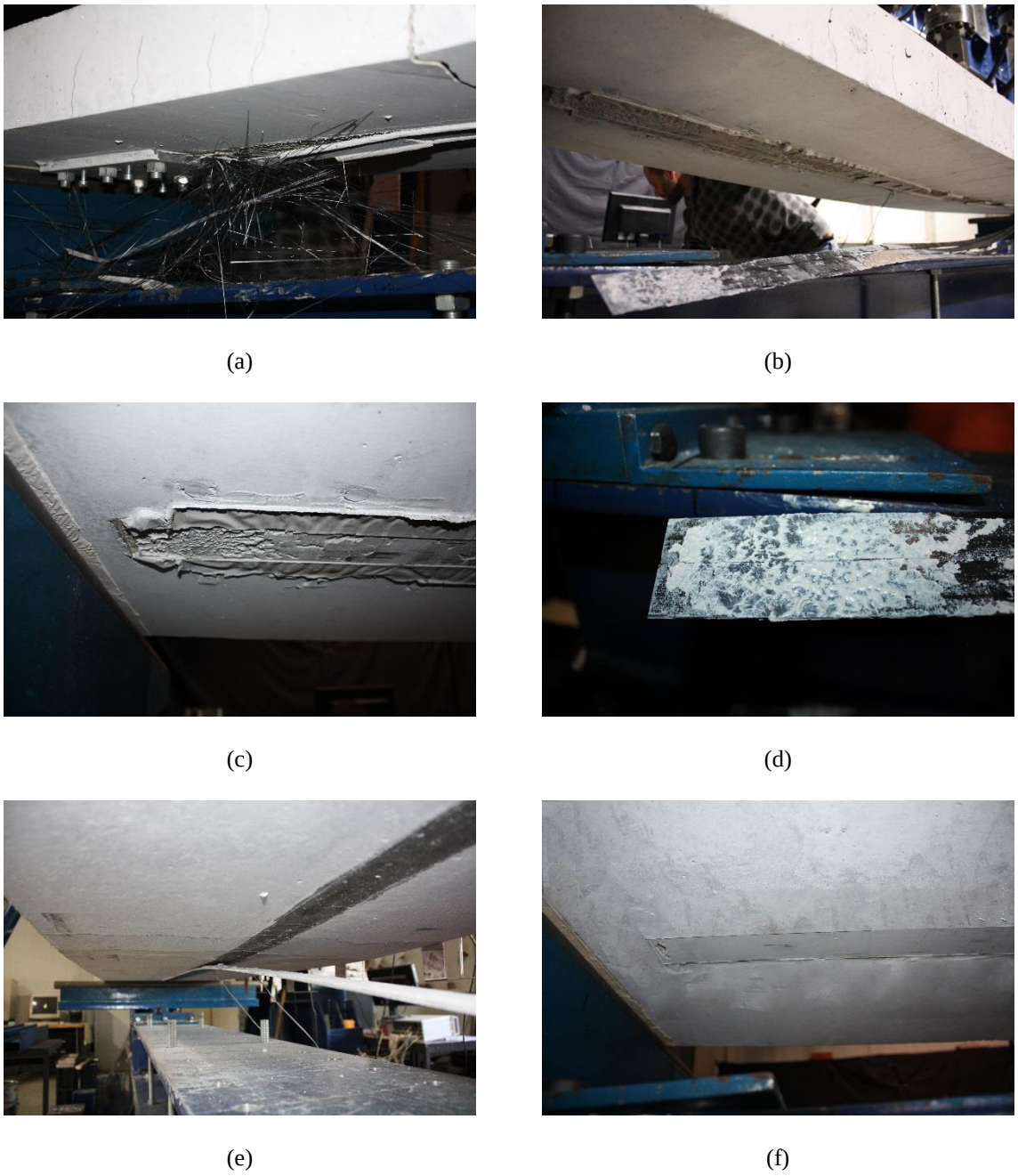

Fig. 12: Typical failure modes: (a) FRP rupture in unidirectional tension (S2_50×1.2_MA); (b) interfacial failure at the epoxy adhesive/CFRP laminate (S2_50×1.2_GA); (c) detail at the anchorage zone (S2_50×1.2_GA); (d) detail of the CFRP strip's extremity (S2_50×1.2_GA); (e) interfacial failure between adhesive and the concrete (S1_50×1.4_EBR); (f) interfacial failure amongst the adhesive and the CFRP strip (S2_50×1.2_EBR).